NON-LINEAR FORCE-FREE MAGNETIC FIELD MODELLING FOR VIM ON SO.

T. Wiegelmann, S. K. Solanki, L. Yelles, and A. Lagg

Max-Planck-Institut für Sonnensystemforschung, 37191 Katlenburg-Lindau, Germany

ABSTRACT

The aim of this work is to investigate how photon noise and errors in the retrieval of solar magnetic parameters from measured Stokes profiles influences the extrapolation of nonlinear force-free coronal magnetic fields from photospheric vector magnetograms. To do so we use a nonlinear force-free extrapolation code based on an optimization principle. The extrapolation method has been extensively tested and applied to data from various telescopes. Here we apply the code to artificial vector magnetograms obtained from 3-D radiation-MHD simulations. As a reference case we compute the coronal magnetic field from an ideal magnetogram and compare the result with more realistic magnetograms based on simulated Solar Orbiter/VIM-measurements. We investigate the effect of noise, ambiguities, spatial resolution, inversion mechanism of Stokes profiles etc. We rate the quality of the reconstructed coronal magnetic field qualitatively by magnetic field line plots and quantitatively by a number of comparision metrices, e.g., the vector correlation with the exact solution and how accurate the free magnetic energy is computed. Not surprisingly, instrument effects and noise influence the quality of the nonlinear force-free coronal magnetic field model. The extrapolations from realistic vector magnetograms show a reasonable agreement with the ideal reconstruction, however, and are in particular significantly better than extrapolations based on line-of-sight magnetograms only. High quality VIM data will thus allow reasonably accurate extrapolations that can serve as the basis for magnetic coupling science through a comparison with observations from EUS and EUI.

Key words: sun; corona, magnetic fields, extrapolations; nonlinear force-free.

1. INTRODUCTION

Except for a few individual cases, e.g., in a newly developed Active Region by Solanki et al. (2003), we cannot measure the magnetic field in the solar corona at high resolution directly and we have to rely on extrapolations from photospheric measurements. Recently Wiegelmann et al. (2005b) compared the direct magnetic field measurements by Solanki et al. (2003) with extrapolations from the photosphere. This work revealed the importance of field aligned electric currents for an accurate magnetic field reconstruction and the need for photospheric vector magnetograms as boundary data. A well known problem is that the noise level of the transversal magnetic field measurements is typically more than one order of magnitude higher than for the line-of-sight component. He we investigate, how the extrapolated coronal magnetic field is influenced by instrument effects and noise, which influence the inversion of the measured Stokes profiles.

To do so we use the results of 3D radiation MHD simulations (see Vögler et al. (2005) for details). The particular snapshot considered here her harbour equal amounts of magnetic flux with both polarities. The corresponding artificial Stokes spectra have been previously used by Khomenko et al. (2005b) for the investigation of magnetoconvection of mixed-polarity quiet-Sun regions and compared with measured Stokes profiles in Khomenko et al. (2005a). We compute synthetic lines from these images, add noise and apply VIM-like filters (see Yelles et al. in this volume). Finally we invert these artificial measurements to derive synthetic vector magnetograms, which are then used as boundary conditions for a nonlinear force-free magnetic field extrapolation. We compare the reconstruction from ideal data, taken directly from the MHD simulations, with extrapolations starting from data containing instrument effects and noise.

2. METHOD

We consider different instrument effects within the inversion process of the Stokes profiles.

- Reference (case 1): Data from MHD simulations.
- Case 2: Inversion from ideal Stokes profiles.
- Case 3: Inversion of Stokes profiles after applying a Fabry-Perrot filter with $100m\AA$ width.
- Case 4: In addition to the filter effects noise with a level $10^{-3}I_c$ is added. After inversion this result has significantly (order of magnitude) larger uncertainties in the transverse field.

Proc. of the Second Solar Orbiter Workshop, 16-20 October 2006, Athens, Greece
(ESA SP-641, January 2007)

An additional instrument effect for cases three and four is a four times reduced spatial resolution.

For the MHD reference case we get B_x, B_y, B_z in the photosphere. For the cases (2-4) we get the total magnetic field strength $B = |\mathbf{B}|$, the inclination angle θ and the azimuth ϕ.

To compute a nonlinear force-free coronal magnetic field from this data we do the following steps:

- Transform B, θ and ϕ to B_x, B_y, B_z on the photosphere.
- Preprocess the vector magnetogram (B_x, B_y, B_z).
- Compute a nonlinear force-free coronal magnetic field from the preprocessed vector magnetogram.
- Compare the result with the reference field.

We explain these steps in the following.

2.1. Transformation of B, θ, ϕ to (B_x, B_y, B_z) on the photosphere.

Transformation equations:

$$B_x = B\sin\theta\cos\phi \quad (1)$$
$$B_y = B\sin\theta\sin\phi \quad (2)$$
$$B_z = B\cos\theta \quad (3)$$

The inclination angle is in the range $\theta = 0\ldots180$ and the azimuth is $-90\ldots90$. The azimuth still contains the 180^o ambiguity which has to be removed before we proceed. The 180^o ambiguity has been removed by minimizing the angle to the exact solution. This possibility does, of course, not exist for real data and we try also to remove the ambiguity by minimizing the angle to a corresponding potential field. The minimum energy method Metcalf (1994) is more sophisticated, but it is outside the scope of this paper to deal with methods of removing the 180^o ambiguity in detail.

In Table 1 we provide the linear Pearson correlation coefficient of the inverted vector magnetogram with the original MHD result. We provide the correlation coefficient for different methods of ambiguity removal (minimize angle to reference field, minimize angle to potential field, not remove the ambiguity). As one can see in Table 1 the performance for the second and third possibility is very poor and we proceed further only with the first choice. We show the resulting vector magnetograms in Figure 1, where the reference case is at the top and the inversion cases 2-4 are in rows 2-4. Figure 1 and Table 1 show that the line-of-sight photospheric magnetic field B_z is much closer to the original than the transversal components of the photospheric magnetic field.

2.2. Preprocessing

The preprocessing routine has been described in detail in Wiegelmann et al. (2006) and we outline only the main features here. The reason why preprocessing of measured photospheric vector magnetograms is necessary is the following. A problem is that measurements of the photospheric magnetic vector field contain inconsistencies and noise. In particular the transversal components (say Bx and By) of current vector magnetographs have their uncertainties, as seen, e.g., in the bottom panel of Figure 1 and in Table 1. Furthermore the magnetic field in the photosphere is not necessarily force-free and often not consistent with the assumption of a force-free field above. Aly (1989) provided criteria that photospheric boundary data have to fulfill in order to be suitable for a force-free extrapolation of the coronal magnetic field above the magnetogram. We developed a preprocessing procedure to drive the observed non force-free data towards suitable boundary conditions for a force-free extrapolation.

To do so we minimize a 2D functional:

$$L = \mu_1 L_1 + \mu_2 L_2 + \mu_3 L_3 + \mu_4 L_4 \quad (4)$$

where

$$\begin{aligned}
L_1 &= \left[\left(\sum_p B_x B_z\right)^2 + \left(\sum_p B_y B_z\right)^2 \right. \\
&\quad \left. + \left(\sum_p B_z^2 - B_x^2 - B_y^2\right)^2\right] \\
L_2 &= \left[\left(\sum_p x\left(B_z^2 - B_x^2 - B_y^2\right)\right)^2 \right. \\
&\quad + \left(\sum_p y\left(B_z^2 - B_x^2 - B_y^2\right)\right)^2 \\
&\quad \left. + \left(\sum_p yB_xB_z - xB_yB_z\right)^2\right] \\
L_3 &= \left[\sum_p \left(B_x - B_{xobs}\right)^2 + \sum_p \left(B_y - B_{yobs}\right)^2 \right. \\
&\quad \left. + \sum_p \left(B_z - B_{zobs}\right)^2\right] \\
L_4 &= \left[\sum_p \left(\Delta B_x\right)^2 + \left(\Delta B_y\right)^2 + \left(\Delta B_z\right)^2\right] \quad (5)
\end{aligned}$$

The surface integrals are here replaced by a summation $\sum_p$ over all grid nodes p of the bottom surface grid and the differentiation in the smoothing term is achieved by the usual 5-point stencil for the 2D-Laplace operator. Each constraint L_n is weighted by a yet undetermined factor μ_n. The first term (n=1) corresponds to the force-balance condition, the next (n=2) to the torque-free condition. The following term (n=3) ensures that the

optimized boundary condition agrees with the measured photospheric data and the last terms (n=4) controls the smoothing. The 2D-Laplace operator is designated by Δ.

The aim of our preprocessing procedure is to minimize L so that all terms L_n if possible are made small simultaneously. As result of the preprocessing we get a data set which is consistent with the assumption of a force-free magnetic field in the corona but also as close as possible to the measured data within the noise level.

2.3. Extrapolation of nonlinear force-free fields.

Force-free coronal magnetic fields have to obey the equations

$$(\nabla \times \mathbf{B}) \times \mathbf{B} = \mathbf{0}, \quad (6)$$

$$\nabla \cdot \mathbf{B} = 0. \quad (7)$$

Wheatland et al. (2000) proposed an optimization principle to solve these equations, which has been generalized by Wiegelmann (2004). We define the functional

$$L = \int_V \left[w_a \, B^{-2} \, |(\nabla \times \mathbf{B}) \times \mathbf{B}|^2 + w_b \, |\nabla \cdot \mathbf{B}|^2 \right] \, d^3x, \quad (8)$$

where w_a and w_b are weighting functions. It is obvious that (for $w_a, w_b > 0$) the force-free equations (6-7) are fulfilled when L equals zero. We minimize the functional (8) numerically as explained in detail in Wiegelmann (2004). The program is written in C and has been parallelized with OpenMP. The code has been applied to vector magnetograph data from the German Vacuum Tower Telescope (VTT) in Wiegelmann et al. (2005b,a) and to data from the Solar Flare Telescope (SFT) in Wiegelmann et al. (2006)

3. RESULTS

3.1. Qualitative comparison

Here we concentrate on the results of the 3D magnetic field reconstruction. Figure 2 shows some magnetic field lines for the reference field and the three inversion cases. First we see that magnetic field lines with footpoints close to the boundary of the magnetogram are not well reconstructed for the cases 2-4. Some near-boundary closed loops in the reference case even occur as open field lines in the reconstructed cases. The poor quality of any magnetic field reconstruction method close to the boundaries of a magnetogram is well known, see, e.g., Wiegelmann et al. (2005b). The reason is, that the unknown magnetic field outside the field-of-view influences the magnetic field in the computational domain. Any assumption regarding these fields are a mere guess and a meaningful magnetic field reconstruction, which is not biased by assumptions regarding the lateral boundary conditions, is only possible for regions far from the boundaries of the computational domain. In other words, the measured photospheric magnetic field vector should include a sufficiently large field-of-view, which includes a reasonably large skirt around the region of interest.

Field lines with both footpoints well inside the magnetogram seem to be reasonably reconstructed for the ideal inversion case 2. The overall magnetic field topology is visible as well for cases 3 and 4, which contain instrument effects due to limited wavelength sampling of the spectral line and for case 4 also noise. A visual inspection of figure 2 shows a larger deviation from the original reference field, however. In the following we introduce several figures of merit to evaluate the performance of the reconstruction quantitatively.

3.2. Figures of merit

Table 2 contains different measures which compare our reconstructed field for cases 2-4 with the reference field. These measures have been introduced by Schrijver et al. (2006) to compare a vector field $\mathbf{b}$ with a reference field $\mathbf{B}$.

- Column 2: Vector correlation:

$$C_{\rm vec} = \sum_i \mathbf{B_i} \cdot \mathbf{b_i} / \left(\sum_i |\mathbf{B_i}|^2 \sum_i |\mathbf{b_i}|^2 \right)^{1/2}, \quad (9)$$

- Column 3: Cauchy-Schwarz inequality

$$C_{\rm CS} = \frac{1}{N} \sum_i \frac{\mathbf{B_i} \cdot \mathbf{b_i}}{|\mathbf{B_i}||\mathbf{b_i}|}, \quad (10)$$

  where N is the number of vectors in the field.

- Column 4: Normalized vector error

$$E_{\rm N} = \sum_i |\mathbf{b_i} - \mathbf{B_i}| / \sum_i |\mathbf{B_i}|, \quad (11)$$

- Column 5: mean vector error

$$E_{\rm M} = \frac{1}{N} \sum_i \frac{|\mathbf{b_i} - \mathbf{B_i}|}{|\mathbf{B_i}|}. \quad (12)$$

- Column 6: total magnetic energy of the reconstructed field normalized with the energy of the reference field

$$\epsilon = \frac{\sum_i |\mathbf{b_i}|^2}{\sum_i |\mathbf{B_i}|^2}. \quad (13)$$

The two vector fields agree perfectly if $C_{\rm vec}, C_{\rm CS}$ and ϵ are unity and if $E_{\rm N}$ and $E_{\rm M}$ are zero.

3.3. Quantitative comparison

Table 2 contains the quantitative comparison measures as introduced in section 3.2. We compare the reference field

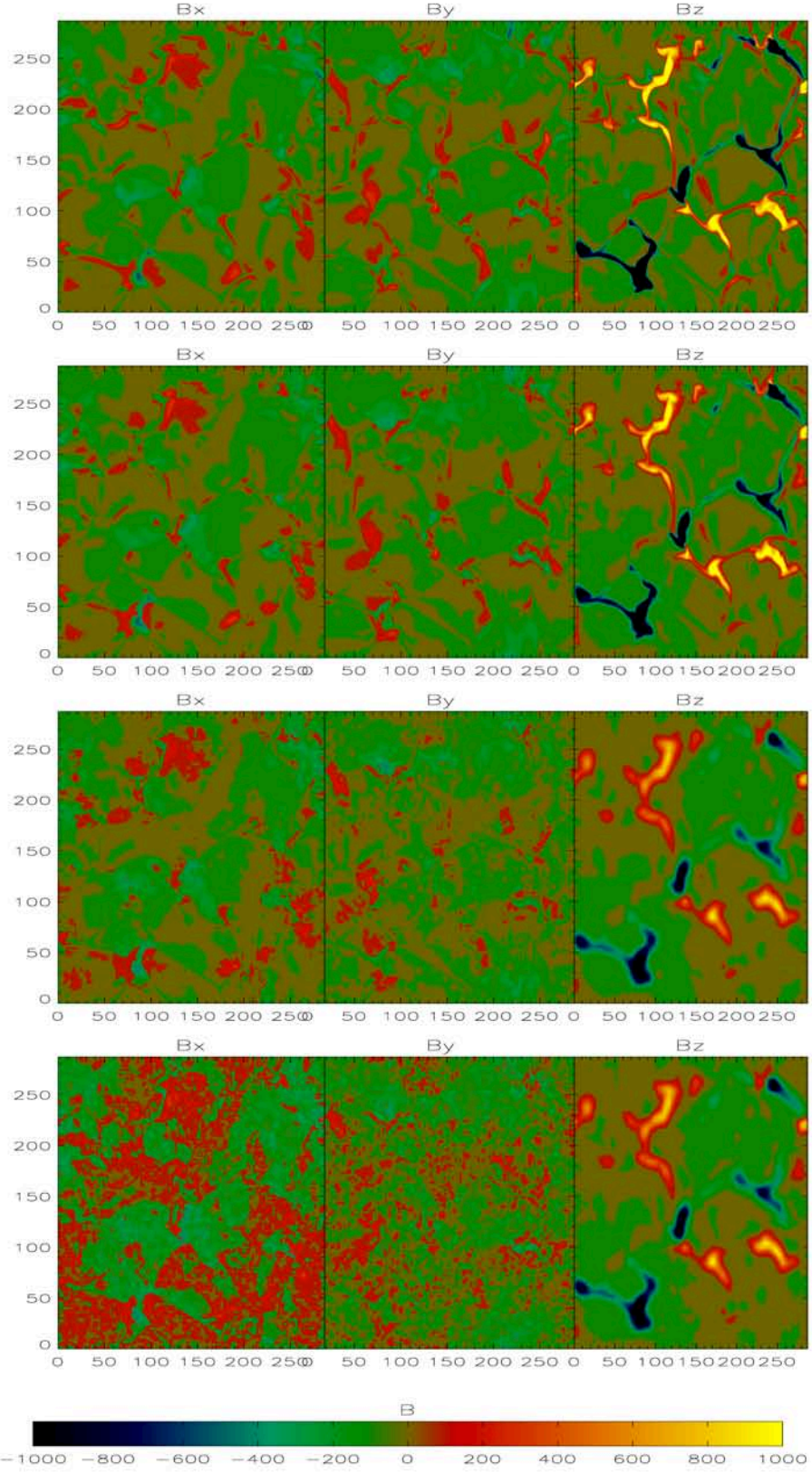

Figure 1. Top: Original magnetogram from the MHD simulations. Row 2-4: Inversions for Cases 2, 3, 4. Please note that the data have been rebinned for cases 3 and 4 for a better comparison.

Table 1. We compare the linear Pearson correlation coefficient of the reference vector magnetogram with the inversion. We removed the 180^o *ambiguity by minimizing the angle to the reference field (column 2-4), a potential field (column 5-7) and without removing the ambiguity (column 8-10). The ambiguity removal does of course not influence the line-of-sight magnetic field component* B_z.

	Ambi ref			Ambi pot			not removed		
Model	B_x	B_y	B_z	B_x	B_y	B_z	B_x	B_y	B_z
Reference	1	1	1	1	1	1	1	1	1
Potential	0.34	0.12	0.97						
Case 2	0.89	0.88	0.97	0.40	0.17	0.97	−0.07	0.05	0.97
Case 3	0.79	0.69	0.85	0.30	0.04	0.85	−0.06	0.09	0.85
Case 4	0.67	0.53	0.85	0.22	0.02	0.85	−0.02	0.00	0.85

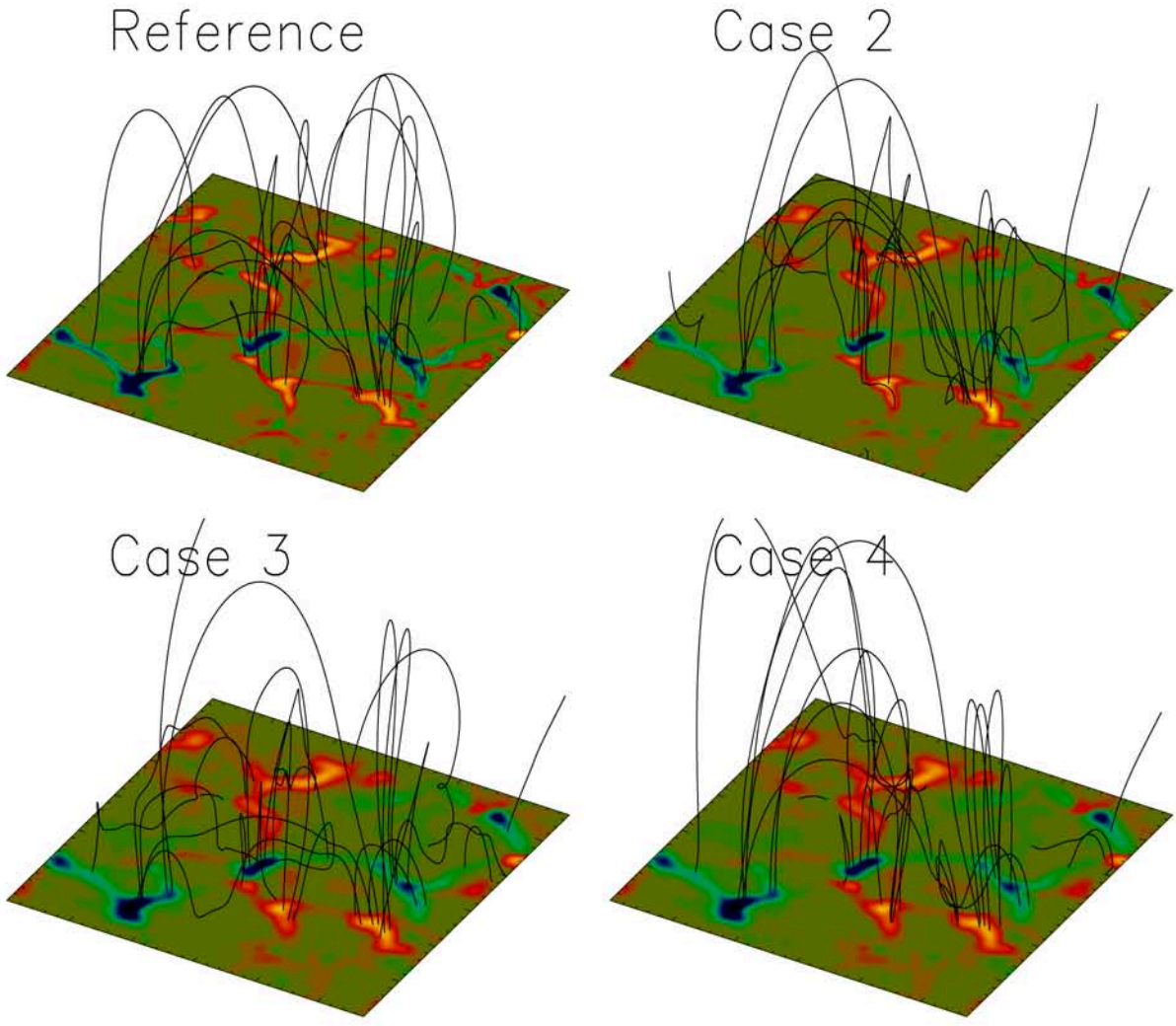

Figure 2. Magnetic field line plots for the reference field and the three inversion cases. The color coding corresponds to the magnetic field strength on the photosphere.

Table 2. We compare different figures of merit of the 3D reconstruction for different cases.

	C_{vec}	C_{CS}	E_N	E_M	ϵ
Reference	1	1	0	0	1
Potential	0.68	0.92	0.51	0.26	0.64
Ideal	0.95	0.98	0.22	0.16	1.05
Filter	0.88	0.97	0.34	0.22	0.88
Filter+Noise	0.84	0.97	0.36	0.22	0.78

with a potential field and the results of cases 2-4. The reconstruction from ideal Stokes profiles give the best agreement with the original reference field for all comparison metrics. A reconstruction from Stokes-profiles taken with a Fabry-Perrot filter (Case 3, forth row in table 2) is less accurate. In particular the values for the vector correlation and the magnetic energy content are significantly worse than for an ideal inversion. For Stokes profiles with noise (Case 4, fifth row in table 2) the comparison figures indicate a further quality loss of the reconstructed coronal magnetic field. We have also to keep in mind, that the inversion of the Stokes profiles for cases 3 and 4 has been carried out with a four times lower spatial resolution, which was comparable with the expected resolution of the VIM-instrument. In particular the deviation (too low) of the magnetic energy for these cases might well be significantly influenced by the resolution effects, as small scale magnetic fields and electric currents are not resolved. We are planning to investigate the influence of resolution effects, different filters and noise levels in more detail in a future work. Despite the cumulative error sources of instrument effects, noise and low resolution for cases 3 and 4, a corresponding nonlinear force-free reconstruction provides a much better agreement with the reference field than a potential field reconstruction.

4. CONCLUSIONS

Our investigations revealed by which amount instrument effects, noise and a limited spatial resolution influence the quality o a nonlinear force-free reconstruction of the coronal magnetic field vector. But even for very noisy data a nonlinear force-free extrapolation is way more accurate than a potential field reconstruction. Potential fields can be reconstructed from the photospheric line-of-sight component alone and do not require knowledge regarding the transversal photospheric magnetic field at all. Nonlinear force-free models require the transversal photospheric magnetic field and lead to an improved reconstruction result, even if the measurement error of this component is relatively high.

ACKNOWLEDGMENTS

We are greatly indebted to R. Cameron, M. Schüssler and A. Vögler for providing us with the analyzed numerical simulation snapshot. The work of T. Wiegelmann was supported by DLR-grant 50 OC 0501.

REFERENCES

Aly, J. J. 1989, Sol. Phys., 120, 19

Khomenko, E. V., Martínez González, M. J., Collados, M., et al. 2005a, A&A, 436, L27

Khomenko, E. V., Shelyag, S., Solanki, S. K., & Vögler, A. 2005b, A&A, 442, 1059

Metcalf, T. R. 1994, Sol. Phys., 155, 235

Schrijver, C. J., Derosa, M. L., Metcalf, T. R., et al. 2006, Sol. Phys., 235, 161

Solanki, S. K., Lagg, A., Woch, J., Krupp, N., & Collados, M. 2003, Nature, 425, 692

Vögler, A., Shelyag, S., Schüssler, M., et al. 2005, A&A, 429, 335

Wheatland, M. S., Sturrock, P. A., & Roumeliotis, G. 2000, ApJ, 540, 1150

Wiegelmann, T. 2004, Sol. Phys., 219, 87

Wiegelmann, T., Inhester, B., Lagg, A., & Solanki, S. K. 2005a, Sol. Phys., 228, 67

Wiegelmann, T., Inhester, B., & Sakurai, T. 2006, Sol. Phys., 233, 215

Wiegelmann, T., Lagg, A., Solanki, S. K., Inhester, B., & Woch, J. 2005b, A&A, 433, 701